Estimation of deformation behavior of TRIP steels - smooth/ringed-notched specimens under monotonic and cyclic loading

Tomita, Yoshihiro

Shibutani, Yoji

ESTIMATION OF DEFORMATION BEHAVIOR OF TRIP STEELS －SMOOTH/RINGED-NOTCHED SPECIMENS UNDER MONOTONIC AND CYCLIC LOADING－

Yoshihiro Tomita* and Yoji Shibutani**

***Graduate School of Science and Technology, Kobe University,**
Nada Kobe Japan 657-8501
****Graduate School of Engineering, Osaka University**
Suita Osaka Japan 565-0876

Abstract

Uniaxial tension tests were performed under a constant strain rate and various environmental temperatures from 77K to 373K to identify the concrete form of the constitutive equation for TRIP steels. To elucidate the dependence of the martensitic transformation on the nonuniform deformation and to validate the proposed constitutive equation, the volume fraction of the martensite phase is predicted and measured using computational simulation and experimental procedures, respectively, for the uniaxial tension of bars with a ringed notch. The good correspondence between the local volume fraction of the martensite phase around the notch obtained by both methods verifies the validity of the proposed constitutive equation for the nonuniform deformation behavior. Subsequently, the computational simulations were performed to elucidate the deformation behavior of ringed-notched bars under compression and that of smooth/ringed-notched bars under cyclic loading.

1. Introduction

Martensitic transformation of transformation-induced plasticity (TRIP) steel is observed during large deformation in the low-temperature range. Owing to the duplex phase of austenite and martensite, the TRIP steel is functionally improved in its ductility and fracture toughness. However, strain and temperature effects on the deformation behavior and the microscopic transformation mechanism are quite complicated, and it may be very difficult to determine a method for the improvement of the mechanical properties merely through experiments. To date, the constitutive equation accounting for the temperature and strain effect on the martensitic transformation (Olson and Cohen 1975) and its generalization to account for the stress state (Stringfellow et al. 1992), strain rate sensitivity (Tomita and Iwamoto 1995a), and the stress state for stacking fault energy (Iwamaoto et al.1998) have been proposed and computational simulations have been conducted to exemplify the transformation behavior and the mechanisms in order

to improve the mechanical properties through the forming processes. For the transformation behavior which is very sensitive to the orientation of the crystalline direction, however, the validity and limitation of the applicability of the constitutive equation should be examined. In particular, the predictability of the whole deformation behavior, including the macroscopic stress-strain relation and local distribution of the martensitic phase based on the developed constitutive equation, has not been fully verified yet.

In this study, SUS304 steel, which is a typical TRIP steel, is employed in the experiments. Through precise tension tests conducted under the environmental temperatures of 77K to 373K, the refinement of the constitutive equation and its identification is done. Subsequently, the predictability of the computational simulation is checked against the experimentally estimated stress strain relations and the distribution of the volume fraction of the martensitic phase. A specially established experimental method that uses the master curve of the volume fraction of martensite vs microhardness is employed for the estimation of the local distribution of the martensite phase over the cross section of a bar with a ringed notch under tension at an environmental temperature of 77K. The results are compared with those obtained by computational simulation, and the validity and the limitation of the computational simulation are discussed. Furthermore, the computational method thus established is applied to the prediction of the deformation behavior of smooth/ringed-notched bars deformed under monotonic compressive loading and cyclic loading.

2. Constitutive Equation of TRIP Steels

Olson and Cohen [1975] established a model for strain-induced martensitic transformation kinetics which can express the temperature dependence of the transformation phenomena. This phenomenological model was constructed under the assumption that the transformation occurred at the intersection of the shear band in the austenite mother phase with a certain probability. Stringfellow et al. [1992] generalized the Olson and Cohen model so as to include the stress state and the contribution of the martensite phase to the strength. Tomita and Iwamoto [1995a] modified the two models to account for the experimental finding that the mode of the deformation behavior is controlled by the shear band mode as the strain rate increases (Hecker et al. 1982). The rate of increase of the volume fraction of martensite, $\dot{f}^m$, is given by

$$\dot{f}^m = A(1-f^m)\dot{\bar{\varepsilon}}_a^{pslip}, \quad A = \alpha p n \eta \left(f^{sb}\right)^{n-1}\left(1-f^{sb}\right), \qquad (1)$$

where $\dot{\bar{\varepsilon}}_a^{pslip}$ is the equivalent strain rate of slip deformation in austenite, f^{sb} is the

volume fraction of the shear band, p is the probability that an intersection forms a martensitic embryo (Stringfellow et al. 1992; Tomita and Iwamoto 1995a), and n and η are geometric constants. α is a parameter related to the stacking fault energy and is a function of temperature T (Olson and Cohen 1975), strain rate $\dot{\bar{\varepsilon}}_a^{pslip}$ (Tomita and Iwamoto 1995a) and the stress triaxiality parameter $\Sigma = \sigma_{ii} / (3\bar{\sigma})$ (Iwamoto et al. 1998) as

$$\alpha = \left(\alpha_1 T^2 + \alpha_2 T + \alpha_3 - \alpha_4 \Sigma\right)\left(\frac{\dot{\bar{\varepsilon}}_a^{pslip}}{\dot{\varepsilon}_y}\right)^M , \tag{2}$$

where M is the strain rate sensitivity exponent, $\alpha_1 - \alpha_4$ are material parameters and $\dot{\varepsilon}_y$ is the reference strain rate.

Next, with the standard notation of an updated Lagrangian formulation (Tomita et al. 1981, Tomita 1990) the total strain rate $\dot{\varepsilon}_{ij}$ is the rate of stretching tensor and is assumed to be the sum of the elastic component $\dot{\varepsilon}_{ij}^e$ and the plastic component $\dot{\varepsilon}_{ij}^p$. The plastic strain rate $\dot{\varepsilon}_{ij}^p$ is decomposed into the plastic strain rate $\dot{\varepsilon}_{ij}^{pslip}$ induced by slip deformation in austenite and martensite, and $\dot{\varepsilon}_{ij}^{ptrans}$ induced by the transformation. Furthermore, the transformation plastic strain rate is split into a deviatoric part, $\dot{\varepsilon}_{ij}^{pshape}$, related to the shape change, and dilatational part, $\dot{\varepsilon}_{ij}^{pdilat}$, expressing the volume change. Under the assumptions that the strain rate $\dot{\varepsilon}_{ij}^{pshape}$ is considered to be coaxial with deviatoric stress (Stringfellow et al. 1992) and that $\dot{\varepsilon}_{ij}^{pdilat}$ can be expressed in terms of the volume change Δv, which has the value of $0.02 - 0.05$ for austenite steel, the plastic strain rate $\dot{\varepsilon}_{ij}^p$ can be expressed as

$$\begin{aligned}
&\dot{\varepsilon}_{ij}^p = p_{ij}\dot{\bar{\varepsilon}}^p + s_{ij}\Delta v \dot{f}^m \\
&p_{ij} = \frac{3\sigma'_{ij}}{2\bar{\sigma}}, \quad s_{ij} = -p_{ij}\Sigma + \frac{\delta_{ij}}{3} \\
&\dot{\bar{\varepsilon}}^p = \dot{\bar{\varepsilon}}^{pslip} + R\dot{f}^m + \Sigma\Delta v \dot{f}^m ,
\end{aligned} \tag{3}$$

where $\dot{\bar{\varepsilon}}^p$ is the work equivalent measure of the equivalent plastic strain rate with respect to Mises-type equivalent stress $\bar{\sigma}$ and R is the parameter accounting for the magnitude of shape changes and depends on the stress. The constitutive equation for the stress rate can be established by introducing the plastic strain rate in Eqn.(3) into the thermoelastic constitutive equation, as discussed by Tomita et al. [1990].

$$\begin{aligned}
&\overset{\nabla}{S}_{ij} = D_{ijkl}^e(\dot{\varepsilon}_{ij} - \dot{\varepsilon}_{ij}^p) - \beta_{ij}\dot{T} \\
&\beta_{ij} = \frac{\alpha_E}{1-2\nu}\delta_{ij} - \frac{1}{E}\frac{\partial E}{\partial T}\sigma_{ij}
\end{aligned} \tag{4}$$

where $\overset{\nabla}{S}_{ij}$ is the Jaumann rate of the Kirchhoff stress S_{ij} which is identical to Cauchy stress σ_{ij} in the current state, D^e_{ijkl} is the elastic stiffness tensor which contains the elasticity modulus E and Poisson's ratio ν. α_E is the thermal expansion coefficient.

The constitutive equation of a two-phase composite material of austenite with the volume fraction of the martensitic phase of f^m is established in a manner similar to that described by Stringfellow et al. [1992], applying Eshelby's theory (Eshelby 1957). The forward gradient method (Piece et al. 1984) is introduced to improve the computational efficiency.

Since strain-induced transformation is quite sensitive to temperature, the mechanical characteristics of the material induced by transformation are strongly affected by the temperature change caused by the irreversible work. Consequently, thermocoupled analysis (Tomita and Iwamoto 1995a) is essential for the prediction of the deformation behavior of TRIP steel.

To identify the constitutive equation, uniaxial tension tests of SUS304 stainless steel specimens shown in the inset, with the chemical compositions indicated in Appendix 1, have been performed under an average strain rate of $5\times10^{-4}/s$ at environmental temperatures of 373K, 293K, 273K, 253K, 233K, 213K, 153K, 113K and 77K. Figure 1 shows the equivalent stress-plastic strain relations. The black circles in the figure indicate the load maximum point where the instability, in Considere's sense, takes place. After the load maximum point, the nonuniform deformation, i.e., necking, starts with a substantial decrease of the nominal stress. The stress-strain relation for 373K, which is higher than the Md temperature, indicates the stress-strain relation for austenite since the martensitic transformation may not occur. The discussion concerning the improvement of the strengthening mechanism caused by the martensitic transformation and the improvement of the ductility and the design of the forming process have been discussed by Tomita and Iwamoto [1995a, 1995b].

However, the problems associated with the underestimation of stress by the established constitutive equation remains unsolved (Shimizu 1998), which can be attributable to the employed stress-strain relation for the martensitic phase. Due to the difficulty of estimating the stress-strain relation for the pure martensitic phase, the stress-strain relations similar to those for the austenitic phase were employed (Tomita and Iwamoto 1995a); the predictability of the stress-strain relation was poor as shown in Fig.2. Here, as did Takimoto et al. (1985) for the experiments of SUS304, the deformation behavior of the martensitic phase is assumed to be elastic. Based on the comparison between the value of the elasticity modulus for the martensitic phase used by Takimoto et al. [1985] and that for the austenitic phase obtained in the present

experiment, a 10% higher value than that for the austenitic phase was introduced for martensitic phase. For the remaining material parameters required for the developed constitutive equation, the similar procedure (Stringfellow et al. 1992, Tomita and Iwamoto 1995a, Shimizu 1998) has been applied to experimentally obtained data, as indicated in Appendix 2. The corresponding reproduction of the stress-strain relation shown in Fig.2 is quite good and is substantially improved as compared with the former one.

3. Boundary Value Problems and Computational Method

With an updated Lagrangian formulation, the weak form of the equation governing the rate of stress and traction yields the virtual work principle (Hill 1958, Seguchi et al. 1971, Kitagawa et al. 1972),

$$\int_V \left(\dot{S}_{ij} + \sigma_{lj} v_{i,l}\right)\delta v_{i,j} dV = \int_{S_t} \dot{P}_i \delta v_i dS \qquad (5)$$

where $\dot{P}_i$ is the nominal traction rate and δv_i is the virtual velocity satisfying the homogeneous boundary condition over surface S_v.

Meanwhile, the weak form of the energy balance equation for the same body subjected to heat flux $q = -n_i q_i = Q$ on S_q can be established by multiplying the local form of the heat conduction equation (Kishino et al. 1979) by δT, which satisfies the homogeneous boundary condition on S_T, and by integrating over the volume V, as expressed by

$$\int_V \delta T \rho c \dot{T} dV + \int_V \delta T_{,i} \kappa T_{,i} dV = \int_V \delta T \left(w^p - \rho l_m \dot{f}^m\right) dV + \int_{S_q} \delta T Q dS \qquad (6)$$

where c is the specific heat, ρ is the density, κ is the thermal conductivity and l_m is the latent heat due to martensitic transformation. The fraction of irreversible work, $w^p = \sigma_{ij}\dot{\varepsilon}_{ij}^p$, which is converted to heat is in the range of 0.85 to 0.95 for many metals (Taylor and Quinney 1934). The specific heat flux Q depends on the respective boundary conditions.

The numerical procedure uses the finite element method (Tomita 1990, Tomita et al. 1990) developed based on the virtual work principle (5) along with the proposed constitutive equation (4). The finite heat conduction equation is established using the weak form of the energy balance equation (6). Ninety per cent of the irreversible work is assumed to transform into heat. The Houbolt method is used to transform the differential equation into a finite difference equation. The thermo-elasto-plastic analysis is performed such that two finite element equations coupled through irreversible work and the constitutive equation, are decoupled at each time step and then solved in turn. The fixed time step Δt_s is determined such that Δt_s is shorter than the time necessary for an accurate solution.

Figure 3 shows the computational model. Due to symmetric deformation, the deformation behavior has been simulated with the finite element discretization shown in the figure. Each quadrilateral consists of four crossed-triangular axisymmetric elements. Convective boundary conditions with heat-transfer coefficient h are assumed at the surface of the bar, whereas adiabatic boundary conditions are introduced at the two ends.

4. Prediction of Deformation Behavior of Smooth/Ringed-Notched Bars under Monotonic Tension

The estimation of the deformation behavior of smooth/ringed-notched specimens under tension, deformed mainly at 77K with average strain rates of 10^{-5} and $10^{-4}/s$, respectively has been done. In Fig.2, the predicted stress-strain relation at different temperatures are shown. A significant improvement is seen as compared with the former stress-strain relations. Therefore, the predictability of the proposed constitutive equation for uniform deformation has been verified.

Next, to validate the constitutive equation for the nonuniformly deformed body, the experimentally evaluated volume fraction of the martensitic phase and that obtained by finite element simulation using the proposed constitutive equation have been compared. For the experimental evaluation of the local distribution of the martensitic phase for the ringed-notched specimen shown in Fig.3 deformed at the environmental temperature of 77K with a average strain rate of $10^{-5}/s$, a newly developed method that employs the master curves relating the microhardness to the average volume fraction of the martensitic phase in a local sense (Shibutani et al. 1997) was used.

Figure 4 indicates the distribution of the volume fraction of the martensitic phase f^m along the radial direction x. Two different indentation loads are applied for the measurement of micro hardness which is correlated to the volume fraction of martensitic phase. Due to the microscopically nonuniform distribution of the martensitic phase, the experimental results fluctuate. Figure 5 indicates the distribution of the volume fraction of the martensite phase f^m over the cross section near the notch tip. Approximately 12000 points have been measured for $196mN$ indentation load. Although the noise due to the measurement is introduced, it has been clarified that in accordance with the local deformation of the notched bar, the region with a high volume fraction of the martensitic phase emanated from the notch tip spreads at approximately $45°$ from the tension axes, which indicates that the martensitic transformation substantially depends on the slip deformation of the crystals (Venables 1964). Due to the strain localization around the notch tip, a region with low martensitic transformation

can be observed along the ligament direction of the notch root. Furthermore, the results reveal that the nonuniform transformation behavior depends on the crystalline direction in a polycrystal of average grain size, $100\mu m$.

To examine the applicability of the constitutive equation for the prediction of the transformation behavior of TRIP steels, computational simulation has been performed for the specimen modeled by the finite element discretization shown in Fig.3. Figures 4 and 5 indicate the distribution of the volume fraction of the martensitic phase f^m predicted by computational simulation, along with those estimated by an experimental method. Due to the computational simulation with constitutive equation employing volume fraction of martensitic phase, the results can not reflect the local distribution of martensitic phase and therefore, are identical for different indentation loads. Apart from the fluctuation of the distribution of the volume fraction of the martensitic phase along radial direction, a very clear correspondence is seen between the two, which implies the applicability of the constitutive equation for the estimation of the volume fraction of the martensite phase created by highly nonuniform deformation. However, the results also indicate the limitation of this computational simulation for problems with highly localized deformation behavior. Therefore, a different type of transformation model which enables the estimation of the local martensite phase (Cherkaoui 1998) and accounts for the characteristic feature of the grains (Peirce et al. 1982, Harren 1997, Harder 1999) should be incorporated and ; this will be our future work.

Thus, the proposed method of estimating the local distribution of the volume fraction of the martensitic phase clarifies the validity of the prediction of the average martensitic phase distribution based on the phenomenologically developed constitutive equation, to some extent; hence we will further discuss the deformation behavior of smooth/ringed-notched specimens under cyclic deformation behavior.

5. Prediction of Deformation Behavior of Smooth/Ringed-Notched Specimens under Cyclic Loading

In order to investigate the deformation behavior of TRIP steels under cyclic loading, the computational simulation of smooth bars deformed under cyclic loading with and without prestrain at environmental temperatures of 77K and 293K has been performed. The temperature 77K corresponds to the lowest temperature achieved by cooling with liquid nitrogen with the maximum volume fraction of the martensitic phase, and 293K is for the case with maximum ductility (Tomita and Iwamoto 1995b) in our experiments. Three different strain amplitudes, 0.02, 0.03 and 0.04, were selected

for the simulation.

Figure 6 shows the stress-strain relations under cyclic loading at 77K and 293K with a strain amplitude of 0.02. Due to the martensitic transformation, rapid hardening, which causes an increase of the stress amplitude, and monotonic decrease in the width of the hysteresis loop with respect to strain are observed. Eventually the elastic cyclic loading can be approached in the case of low temperature, whereas plastic deformation remains in the case of high temperature and the deformation is mainly consumed in the austenitic phase. Figure 7 indicates the volume fraction of the martensitic phase and the stress amplitude with respect to the applied number of cycles. As expected, a rapid saturation of the volume fraction of the martensitic phase is attained with a larger amplitude of strain at a lower temperature, which is manifested as the saturation of the stress amplitude at a lower number of cycles. On the other hand, the saturation of the stress amplitude has not yet been observed at 40 cycles of loading in the high temperature range. The results obtained are quite similar to those experimentally obtained for SUS304 (Shirasawa et al. 1993, Yokotsuka and Ikegami 1999). It should be noted that the saturation value of the volume fraction of the martensitic phase for cyclic loading is higher than that for monotonic tension, which is attributable to the different probability of martensitic transformation at the intersection of shear bands, as indicated in Eq.(2). Figure 8 indicates the accumulated plastic strain versus number of cycles. The evolution of volume fraction of martensitic phase and the stress amplitude with respect to accumulated plastic strain. The case without prestrain is reproduced well by the experimentally derived relation for the stress amplitude with respect to accumulated plastic strain (Tanaka et al. 1991, Shirasawa et al. 1993), which suggests that the computationally predicted deformation behaviors of TRIP steels under cyclic loading can reproduce those obtained by experiments. However, information concerning material parameters is insufficient to identify the constitutive equation for the employed SUS304 steels in experiments, therefore, we cannot proceed with further quantitative comparisons.

The effect of prestrain on the accumulated plastic strain versus cycle number, volume fraction of the martensitic phase and stress amplitude with respect to the accumulated plastic strain can be seen in Fig.8. The rate of accumulation of plastic strain decreases as the number of cycles increases and asymptotically approaches a specific value which is due to the martensitic transformation of the austenitic phase and is attributable to the identical saturation value of the martensitic phase for the case with different prestrain, as shown in Fig. 8(b). On the other hand, the stress amplitude increases with accumulated plastic strain, whereas, the rate of increase is suppressed

with prestrain. This can be explained by the fact that the fraction of hardening due to martensitic transformation after prestraining decreases as the magnitude of prestrain increases.

Thus, although the quantitative comparison between the computationally predicted results and those obtained experimentally is restricted to the case of monotonic tension, based on the discussion in this section, we can expect that our computational strategy to predict the deformation behavior of TRIP steels may be a valuable tool for clarifying the general feature of deformation under the monotonic, as well as the cyclic, loading process of TRIP steels. The rest of the section is devoted to the cyclic loading process of ringed-notched specimens at an environmental temperature of 77K.

The computational model employed is shown in Fig.3. The typical load-displacement relation for 40 continuous cycles is shown in Fig.9 (a). The corresponding load amplitude versus number of cycles is shown in (b). Since the deformation is localized to the notched region, the saturation of the volume fraction of the martensitic phase is restricted to rather small area where the stress-strain relation is very similar to that shown in Fig.6. Therefore, the asymptotic nature of the load amplitude versus number of cycles can be seen .in the early stage of cycles, and the hysteresis loop in load vs displacement relations is very small and converges very rapidly to the quasi-elastic deformation process. Figure 10 shows the evolution of the volume fraction of the martensitic phase for different numbers of cycles. The area with a high volume fraction of the martensitic phase starts from the notch root and penetrates into the interior of the specimen at approximately 45degrees with respect to the tension axis. This martensitic transformation causes the distribution effect of the deformed region, as indicated in Fig.11(a) which shows the distribution of the equivalent plastic strain. The comparison between the evolution of plastic strain (a) for TRIP steels and (b) for the nontransforming steels, namely, the austenite phase, clearly exhibits the distribution effect. For comparison purpose, Fig. 12 shows the evolution of the volume fraction of the martensitic phase for monotonic (a) tension and (b) compression. Due to the high value of the transforming probability of the intersection site of micro shear bands to a martensitic embryo, the transformation in the case of compression is promoted further than that in the case of tension. Therefore, the evolution of the volume fraction of the martensitic phase under the cyclic loading process is mainly promoted during the compressive loading process. Furthermore, the blunting of the notch root proceeds in the order of tension, cyclic loading and compression, so that the volume fraction of the martensitic phase becomes saturated in the reverse order. For cyclic

loading, further transformation mainly occurs in the austenitic phase during the compressive process. Depending on the local stress and strain distribution, the material points exhibit different histories of deformation, so that the martensitic transformation that affects the change of such stress and strain distribution also contributes to the subsequent transformation process. Therefore, the effects of different types of prestrain and their magnitude on the martensitic transformation must be incorporated in the formulation of the constitutive equation, which is indispensable for accurate prediction of the deformation process of TRIP steels.

6. Conclusion

In this study, by means of precise tension tests conducted at the environmental temperatures of 77K to 373K, the constitutive equation that models for martensitic transformation depending on strain rate, temperature and applied stress system, was established. The computational strategy for the prediction of the deformation behavior of TRIP steels was then developed using the established constitutive equation. Subsequently, through comparison between the computationally predicted stress-strain relation for 77K and 293K, the validity of the proposed constitutive equation in predicting macroscopic nature of deformation behavior was verified. Subsequently, the local distribution of the martensitic phase over the ringed-notched specimen deformed under tension at 77K was predicted computationally and compared with the values obtained by a specially arranged experimental procedure using the microhardness testing device. The good correspondence between the two results confirms the validity of the present computational strategy.

Finally, the computational simulation of the deformation behavior of TRIP steel bars without/with the ringed notch under uniaxial tension at 77K was performed. The effect of temperature, prestrain and amplitude of strain on the deformation behaviors were discussed and the accuracy of the computational results was investigated. Due to the lack of material parameters for the materials employed in the experiments of cyclic loading, the discussion was restricted to a qualitative one; nevertheless the essential feature of the deformation behaviors were reproduced by the computational simulation. Therefore, the clarification of the deformation behavior of the ringed-notched specimen under cyclic loading is expected to reveal the general feature of the deformation behavior of TRIP steels under complex loading.

Further improvement of the constitutive equation incorporating the effect of prestrains and their history is strongly required for future work.

Acknowledgments

Financial support from the Ministry of Education of Japan is gratefully acknowledged. I wish to thank Mr. T. Iwamoto, Research Associate of Hiroshima University, for valuable discussions and graduate students Messrs. T. Ogawa, A. Taniyama, M. Shimizu and H. Sakaue, Kobe University, for assistance with the calculations and experiments.

References

Cherkaoui, M., Berveille, M. and Sabar, H. (1998), "Micromechanical modeling of martensitic transformation induced plasticity (TRIP) in austenitic single crystals", Int. J. Plasticity, Vol.14, 597-626.

Eshelby, J. D. (1957), “The Determination of the Elastic Field of an Ellipsoidal Inclusion, and Related Problems”, Proc. Roy. Soc. Lond., Vol. A241, pp.376-396.

Harder,J. (1999), "A crystallographic model for the study of local deformation processes in polycrystals". Int. J. Plasticity, Vol.15, 605-624.

Harren, S.V. (1997), "Theory of evolution of crystal lattice orientation density and state variables in euler space", Int.J.Plasticity, Vol.13, 59-74.

Hecker, S. S., Stout, M. G., Staudhammer, K. P. and Smith, J. L. (1982), “Effect of Strain State and Strain Rate on Deformation Induced Transformation in 304 Stainless Steel: Part I. Magnetic Measurements and Mechanical Behavior”, Metall Trans A, Vol. 13, pp.619-626

Hill, R. (1958) "A General Theory and Uniqueness and Stability in Elastic-plastic Solids", J. Mech. Phys. Solids, Vol. 8, pp.236-249.

Iwamoto, T., Tsuta, T. and Tomita, Y. (1998), ”Investigation on Deformation Mode Dependence of Strain-Induced Martensitic Transformation in TRIP Steels and Modeling of Transformation Kinetics”, Int. J. Mech. Sci., Vol. 40, pp.173-182.

Kishino, T., Nagaki, S. and Inoue, T. (1979), "On Transformation Kinetics, Heat Conduction, Elastic-plastic Stress During Quenching of Steel", J. S. Materials Sci. Japan, Vol.28, pp.69-76.

Kitagawa, H., Seguchi, Y. and Tomita, Y. (1972), "An Incremental Theory of Large Strain and Large Displacement Problems and Its Finite Element Application", Ing. Arch., Vol. 41, pp.213-224.

Olson, G. B. and Cohen, M. (1975), “Kinematics of Strain-Induced Martensitic Nucleation”, Metall Trans. A, Vol. 6, pp.791-795.

Peirce,D., Asaro,J.R. and Needleman, A. (1982), " An analysis of nonuniform and localized deformation in ductile single crystals", Acta Metall, Vol.30, 1087-1119.

Peirce, D., Shih, C. F. and Needlemen, A. (1984), "A Tangent Modulus Method for Rate Dependent Solids." Computers and Structures, Vol. 18, pp. 875-887.

Seguchi, H., Kitagawa, H., Tomita, Y. and Shindo, A. (1971), "Note on an Incremental Theory of Large Strain and Large Displacement", Memo. Fac. Engng. Kobe Univ., Vol. 17, pp.51-60.

Shibutani, Y., Taniyama, A., Tomita, Y. and Adachi, T. (1997), “Measurement of Local Strain-Induced Martensitic Phase Transformation by Micro-Hardness”, JSMS Japan, Vol. 46, pp.893-899.

Shimizu, M. (1998), Evaluation of strain-induced martensitic phase transformation behavior by micro-hardness and its application to constitutive modeling of TRIP steel, Solid Mechanics Research Laboratory Report, No. 9802 , pp.1-63, (in Japanese).

Shirasawa, H, Ikegami, K, and Niitsu, Y, (1993), Experimental investigation of cyclic plastic deformation of stainless steel 304 at low temperature, Trans. JSME., 59A, 2427 (in Japanese)

Stringfellow, R. G., Parks, D. M. and Olson, G. B. (1992), “A Constitutive Model for Transformation Plasticity Accompanying Strain-induced Martensitic Transformation in Metastable Austenitic Steels”, Acta Metall, Vol. 40, pp.1703-1716.

Takimoto, A., Inoue, T. and Shouda, S. (1985), Relationship between the electrical resistivity and the volume fraction of martensite induced by quenching and deformation, J. Japan Inst. Metals. 49-5, pp.313-319. (in Japanese)

Tanaka, N, Shirasawa, H, Niitsu, Y and Ikegami, K. (1991), Experimental investigation of plastic deformation of SUS304 stainless steel at 77K, Trans JSME., 57, 2775-2781. (in Japanese)

Tomita, Y., Shindo, A, and Kitagawa, H. (1981), Bifurcation and Post Bifurcation Behaviour of Internally Pressurized Elastic-plastic Circular Tubes under Plane Strain Conditions, Int. J. Mech. Sci. Vol. 23, pp.723-732.

Tomita, Y. (1990) Computational Elasto-plasticity, Yokendo, (in Japanese)

Tomita, Y., Shindo, A. and Sasayama, S. (1990), “Plane Strain Tension of Thermo-Elasto-Viscoplastic Blocks”, Int. J. Mech. Sci. Vol. 32, pp.613-622.

Tomita, Y. and Iwamoto, T. (1995a), “Constitutive Modeling of TRIP Steel and Its Application to the Improvement of Mechanical Properties”, Int. J. Mech. Sci., Vol. 37, pp.1295-1305

Tomita, Y and Iwamoto, T. (1995b), “ Computational Simulation of Enhancement of Ductility in TRIP Steels Due to Environmental Temperature Control During Deformation Processes” Proc. Plasticity' 95, pp. 331-334 Gordon and Breach

Taylor, G. I., and Quinney, H. (1934), "The Latent Energy Remaining in a Metal after Cold Working ", Proc. Roy. Soc. London, Vol.A143, pp.307.

Venables, J. A, (1964), The martensitic transformation in stainless steel, Phil. Mag., 7, 35-43

Yokotsuka, T and Ikegami K., (1999), Cyclic plastic deformation at low temperature in liquid nitrogen and room temperature subsequent to pre-strain at low temperature in liquid nitrogen and room temperature, J. Soc. Mat. Sci., Japan, 48, 38-43 (in Japanese)

Figure Captions

Figure 1 Equivalent stress $\bar{\sigma}$ -plastic strain $\bar{\varepsilon}^p$ relations for SUS304 stainless steel deformed with strain rate of $5.0 \times 10^{-4} / s$ under different environmental temperatures of 77-373 K.

Figure 2 Comparison between the experimentally obtained equivalent stress $\bar{\sigma}$ -plastic strain $\bar{\varepsilon}^p$ relations for SUS304 stainless steel deformed with strain rate of $5.0 \times 10^{-4} / s$ and computationally predicted results with (a) constitutive equation of Tomita and Iwamoto (1995a) and (b) present constitutive equation.

Figure 3 Specimen profile and computational model for finite element simulation.

Figure 4 Distribution of volume fraction of martensitic phase f^m along radial direction x estimated using the experimental method with different indentation loads and by computational simulation.

Figure 5 Comparison between distribution of volume fraction of martensite phase f^m estimated experimentally and by computational simulation.

Figure 6 Typical equivalent stress-strain relations for cyclic loading with strain amplitude of 0.02 at environmental temperatures of (a) 77K and (b) 293K.

Figure 7 Evolution of (a) volume fraction of martensitic phase and (b) stress amplitude with respect to applied numbers of loading cycles with different strain amplitudes and environmental temperatures.

Figure 8 Effect of prestrain on (a) accumulated plastic strain, (b) volume fraction of martensitic phase and (c) stress amplitude.

Figure 9 Deformation behaviors of ringed-notched specimens deformed under cyclic loading; (a) load-displacement relations and (b) evolution of the load amplitude.

Figure10 Evolution of volume fraction of martensite phase f^m with cyclic loading.

Figure 11 Distribution of equivalent strain $\bar{\varepsilon}^p$ with number of loading cycles for (a) TRIP steels and (b) hypothetical nontransforming steels, austenite.

Figure 12 Evolution of volume fraction of martensitic phase f^m under monotonic (a) tension and (b) compression.

Appendix 1 Chemical Composition of SUS304 Stainless Steel in wt%

C:0.076, Si:0.45, Mn:1.18, P:0.028, S:0.023, Ni:8.19,
Cr:18.22, Mo:0.06, N:0.0786, Nb:>0.01

Appendix 2 Material and Computational Parameters

Elastic Modulus

$E_a = 215.7 - 0.0692T(GPa)$, $E_m = 237.3 - 0.0692T(GPa)$,

Poisson's ratio

$\upsilon = 0.3$

Evolution of volume fraction of martensitic phase

$$\dot{f}^m = A(1-f^m)\dot{\bar{\varepsilon}}_a^{pslip}$$

$$A = \alpha p n \eta \left(f^{sb}\right)^{n-1}\left(1-f^{sb}\right)$$

$$\alpha = \left(\alpha_1 T^2 + \alpha_2 T + \alpha_3 - \alpha_4 \Sigma\right)\left(\frac{\dot{\bar{\varepsilon}}_a^{pslip}}{\dot{\varepsilon}_y}\right)^M$$

$\eta = 4.5$, $\beta = 2.13$, $M = 0.013$, $\dot{\varepsilon}_y = 5.0\times10^{-4}\ /\ s$

for $T \le 273K$, $\alpha_1 = -2.02\times10^{-4}$, $\alpha_2 = 3.27\times10^{-2}$,
$\alpha_3 = 11.7$, $\alpha_4 = 10.23$

for $T \ge 273K$, $\alpha_1 = 0.0$, $\alpha_2 = -7.92\times10^{-2}$,
$\alpha_3 = 27.1$, $\alpha_4 = 10.23$

Standard deviation 17.0

Mean value –276.0

Stress-strain relation

$$\sigma_0 = \sigma_y + c_1\left\{1.0 - \exp\left(-c_2\bar{\varepsilon}_p\right)\right\}^{c_3},\ \sigma_y = c_4\exp\left(-c_5 T\right)$$

austenite phase

$c_1 = 1861.0$, $c_2 = 0.628$, $c_3 = 0.748$, $c_4 = 660.0$, $c_5 = 0.0027$

martensite phase

$c_1 = 1191.0$, $c_2 = 1.33$, $c_3 = 0.540$, $c_4 = 1056.0$, $c_5 = 0.0013$

Free energy

$g = -T + g_1\Sigma$, $g_1 = 28.7$

Constitutive equation for plastic strain rate

$$\dot{\varepsilon}_{ij}^p = p_{ij}\dot{\bar{\varepsilon}}^p + s_{ij}\Delta v\dot{f}^m$$

$$p_{ij} = \frac{3\sigma'_{ij}}{2\bar{\sigma}},\ s_{ij} = -p_{ij}\Sigma + \frac{\delta_{ij}}{3},\ \dot{\bar{\varepsilon}}^p = \dot{\bar{\varepsilon}}^{pslip} + R\dot{f}^m + \Sigma\Delta v\dot{f}^m$$

$$R = R_0 + R_1\left(\frac{\sigma}{\sigma_y}\right),\ R_0 = 0.02,\ R_1 = 0.02,\ \Delta v = 0.02$$

Material parameters related to heat conduction

$\rho = 0.78\times10^4\,(Kg/m^3)$, $c = 0.46\times10^3\,(J/kg\cdot K)$, $\kappa = 16.3(W/m\cdot K)$

$h = 25.0(W/m^2\cdot K)$, $\alpha_E = 17.3\times10^{-6}/K$, $l_m = -1.50\times10^4\,(J/kg)$

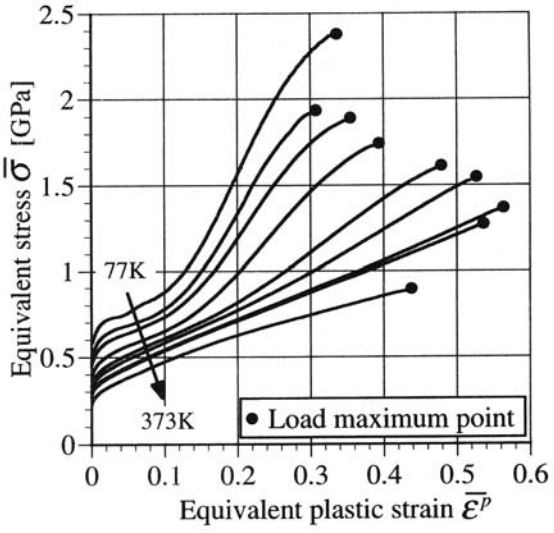

Figure 1.

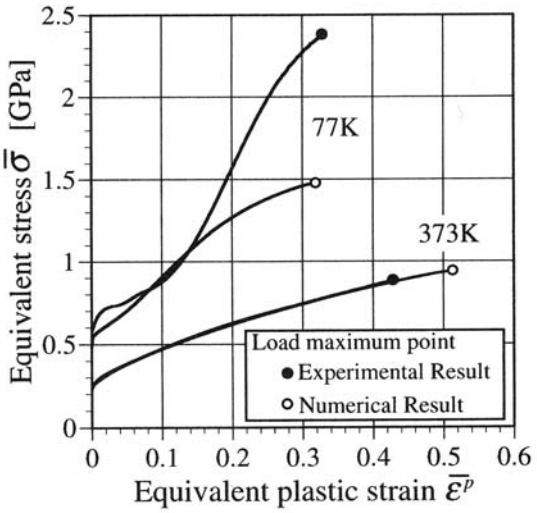

(a)

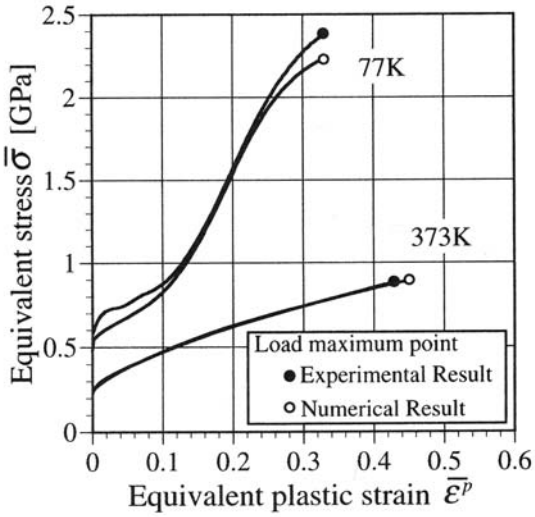

(b)

Figure 2.

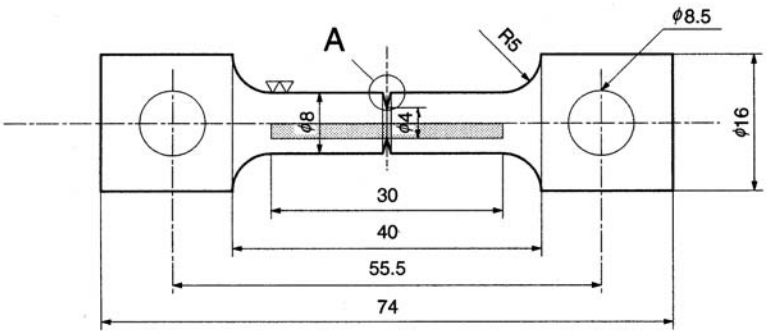

Specimen

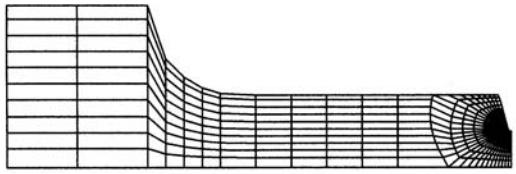

Computational Model

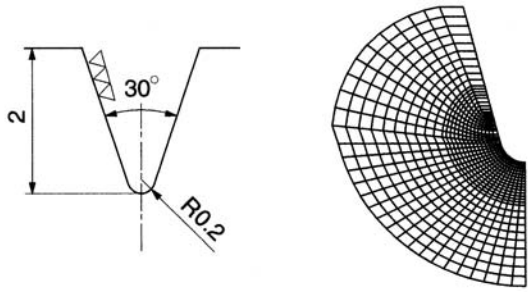

Magnification of A

Figure 3.

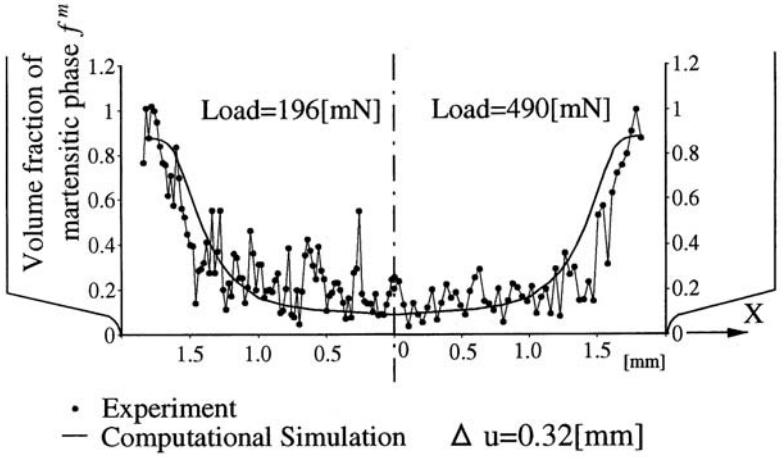

Figure 4.

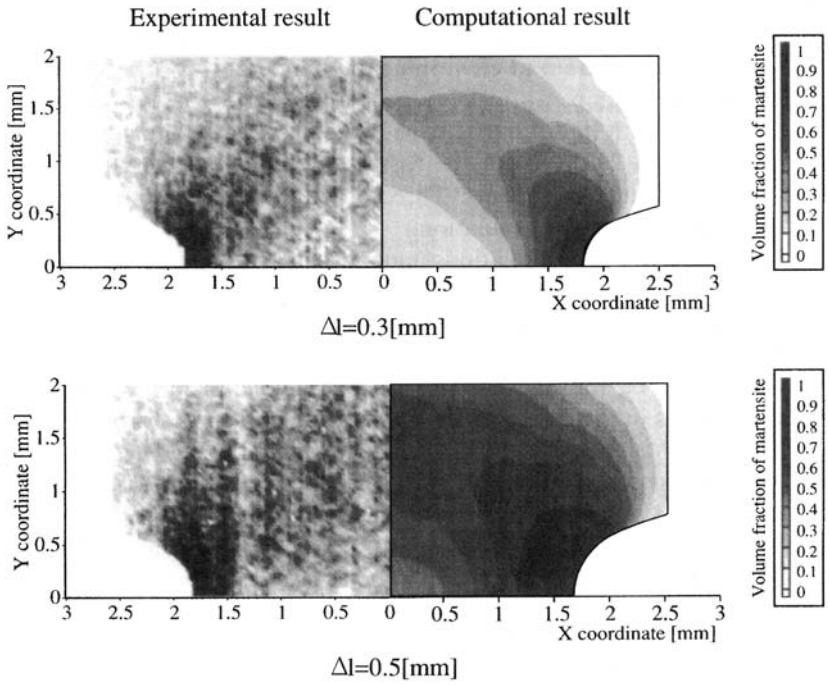

Figure 5.

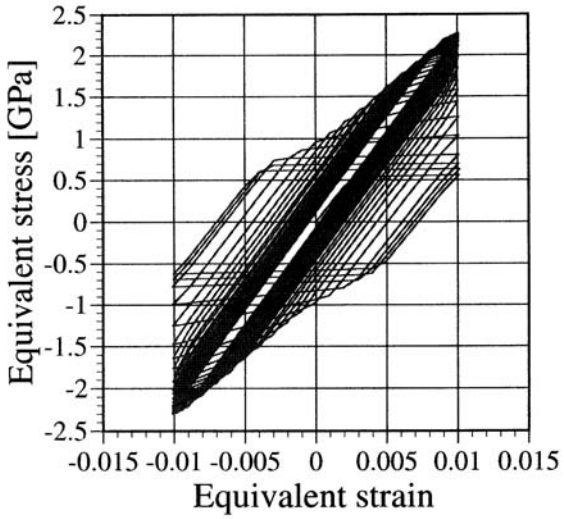

(a) 77K

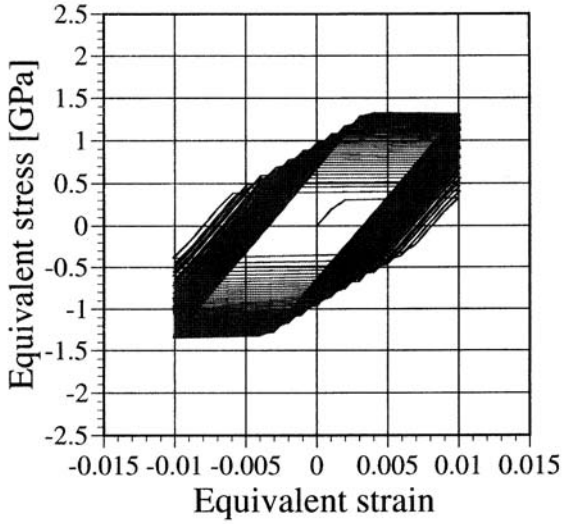

(b) 293K

Figure 6.

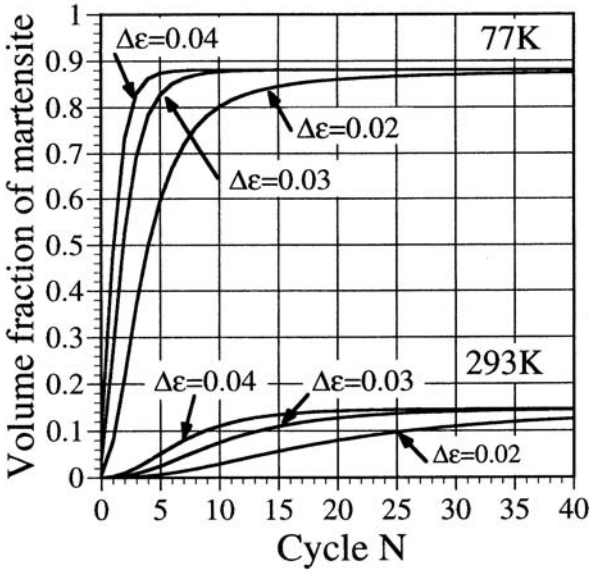

(a)

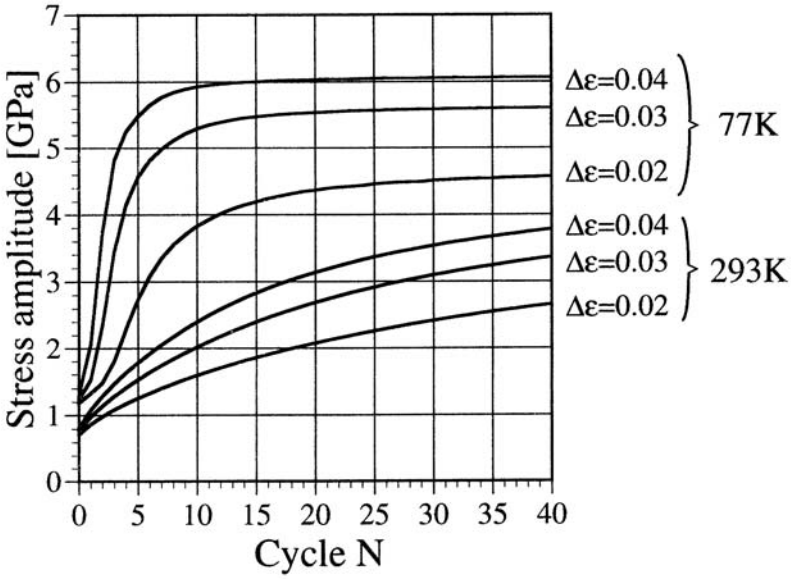

(b)

Figure 7.

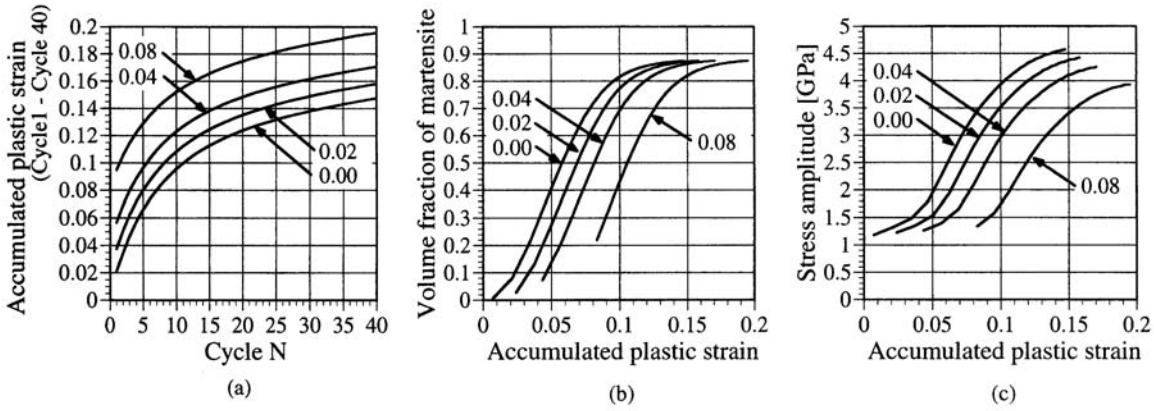

Figure 8.

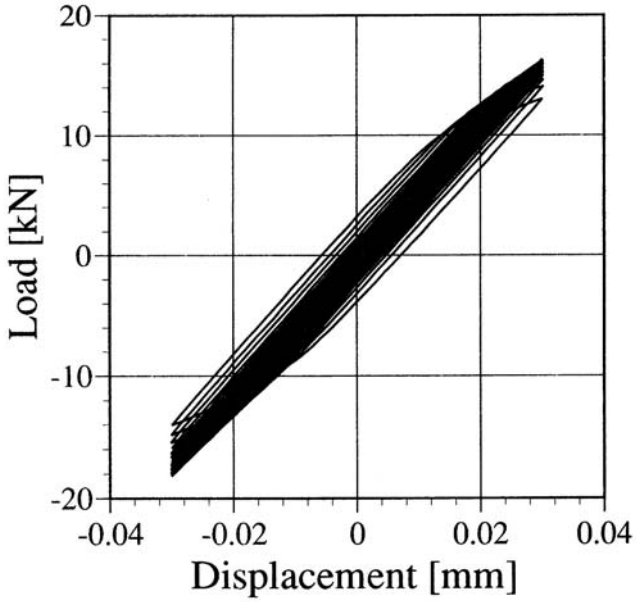
20
10
0
-10
-20
Load [kN]
-0.04
-0.02
0
0.02
0.04
Displacement [mm]

(a)

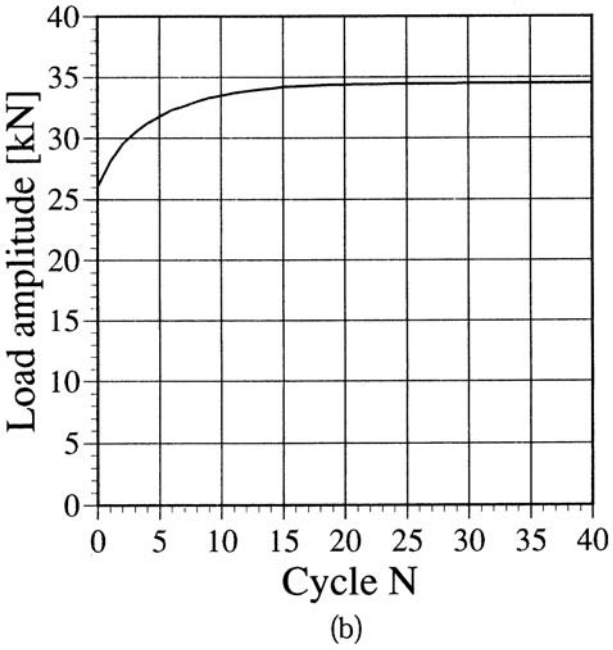
40
35
30
25
20
15
10
5
0
Load amplitude [kN]
0
5
10
15
20
25
30
35
40
Cycle N

(b)

Figure 9.

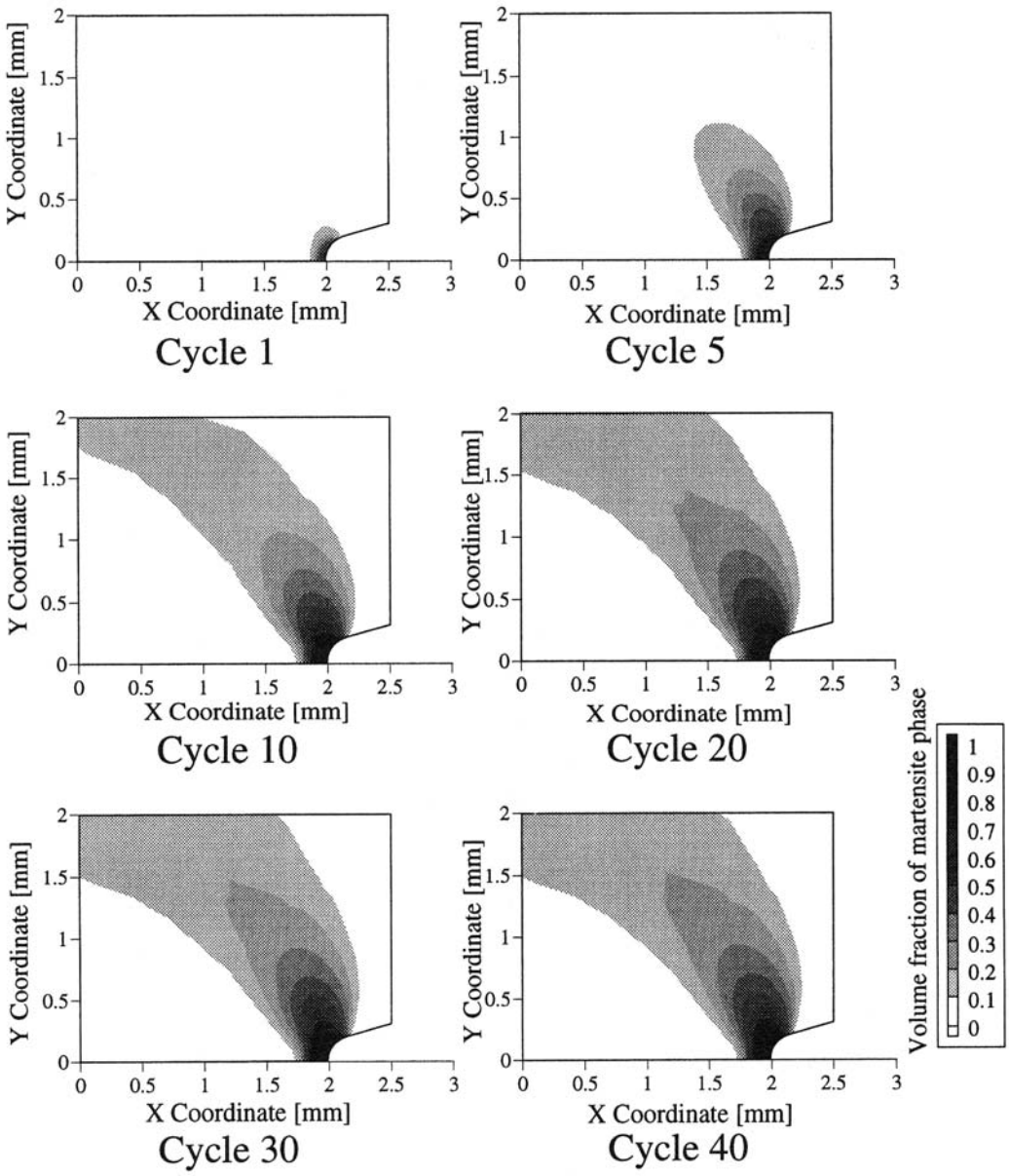
Y Coordinate [mm]
X Coordinate [mm]
Cycle 1
Cycle 5
Cycle 10
Cycle 20
Cycle 30
Cycle 40
Volume fraction of martensite phase
1
0.9
0.8
0.7
0.6
0.5
0.4
0.3
0.2
0.1
0

Figure 10.

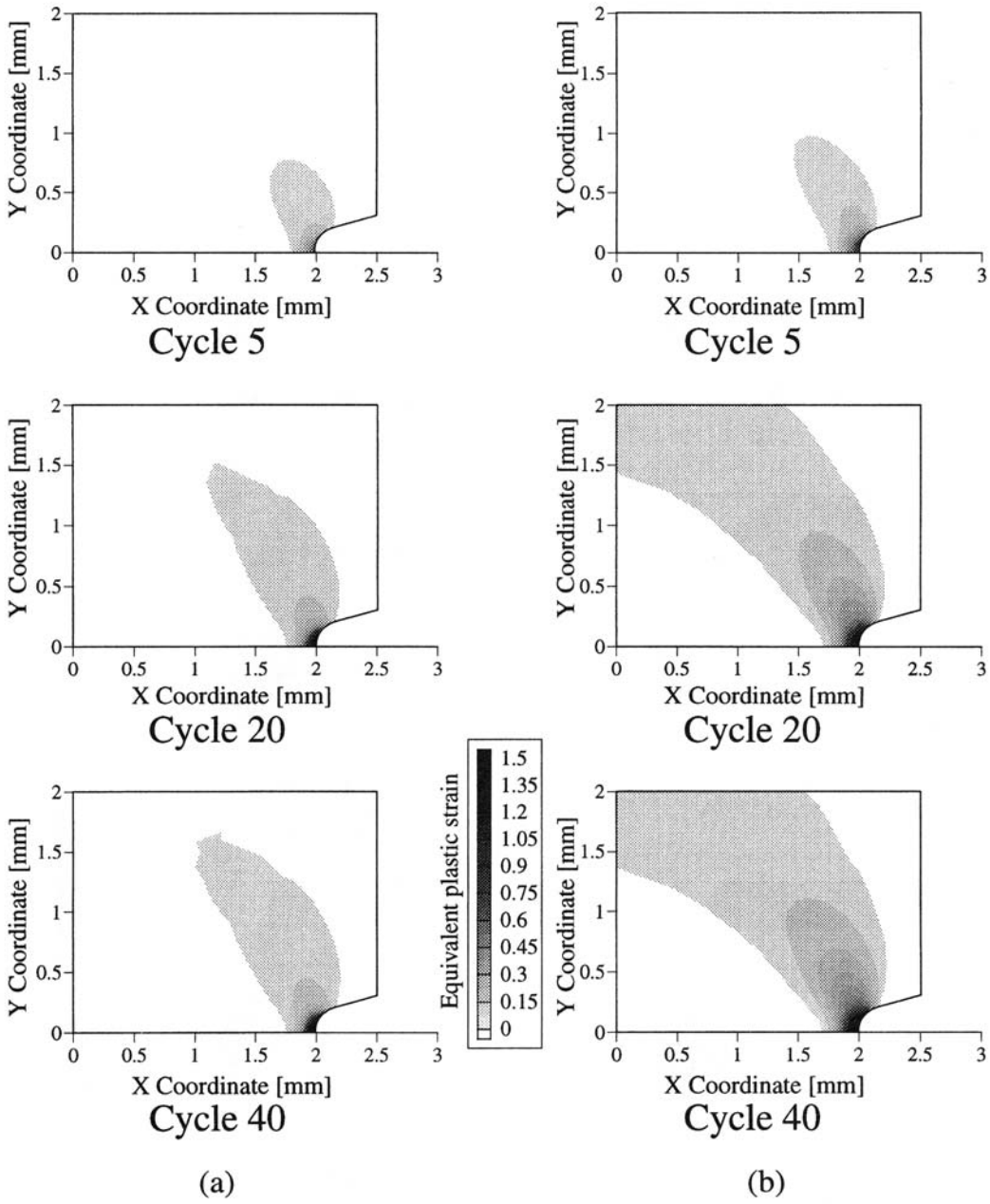
Y Coordinate [mm]
X Coordinate [mm]
Cycle 5
Cycle 20
Cycle 40
Equivalent plastic strain
1.5
1.35
1.2
1.05
0.9
0.75
0.6
0.45
0.3
0.15
0
(a)
(b)

Figure 11.

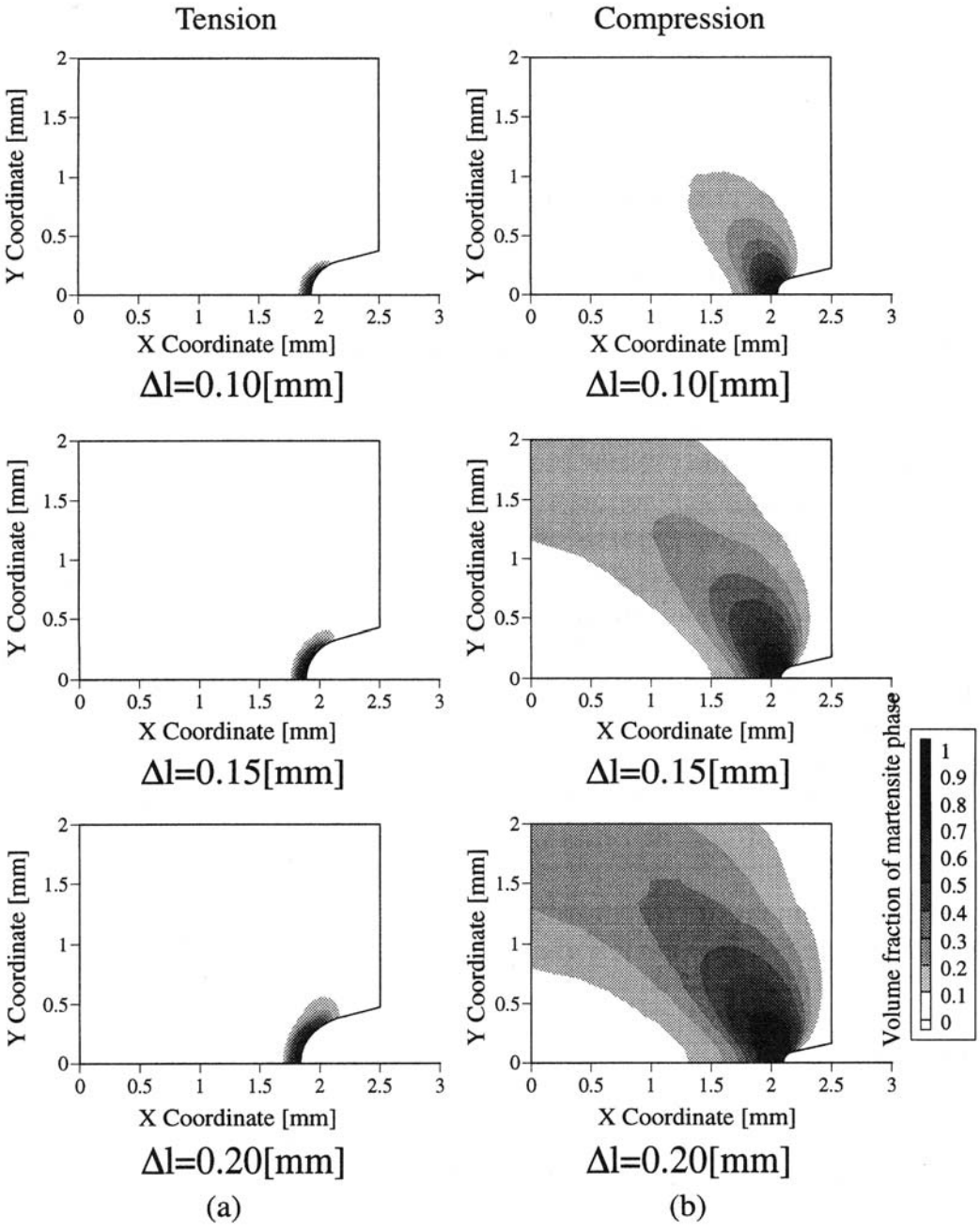
Tension
Compression
Y Coordinate [mm]
X Coordinate [mm]
Δl=0.10[mm]
Δl=0.15[mm]
Δl=0.20[mm]
(a)
(b)
Volume fraction of martensite phase
1
0.9
0.8
0.7
0.6
0.5
0.4
0.3
0.2
0.1
0

Figure 12.